How does a newly-formed drainage divide migrate after a river capture event? Insights from numerical simulations and two natural cases (Yarlung-Yigong, and Dadu-Anning) in the Tibetan Plateau region

Shuang Bian[1], Xibin Tan[2,*], Chao Zhou[1], Feng Shi[1], Yiduo Liu[2]

[1] State Key Laboratory of Earthquake Dynamics, Institute of Geology, China Earthquake Administration, Beijing 100029, China

[2] Key Laboratory of Mountain Hazards and Surface Processes, Institute of Mountain Hazards and Environment, Chinese Academy of Sciences, Chengdu 610041, China

*Corresponding author: Xibin Tan

E-mail address: tanxibin@imde.ac.cn

Key Points:

- A newly-formed drainage divide following a capture event migrates for tens of millions of years, with a decreasing rate over time.
- The Dadu-Anning drainage divide would further migrate ~65–92 km southward to reach a steady state in tens of millions of years.
- The Yarlung-Yigong capture event occurred in the early-middle Cenozoic, which cannot drive the late-Cenozoic enhanced exhumation.

Abstract

Tectonic and/or climatic perturbations can drive drainage adjustment. The capture events, significantly changing the river network topology, are the major events in river network evolution. While they could be identified through field observations and provenance analysis, reconstructing this evolution process and pinpointing the capture time remain challenging. Following a capture event, the steady-state elevation of the captor river will be much lower than that of the beheaded river. Then, the newly-formed drainage divide will migrate towards the beheaded river, a process also known as river-channel reversal. The migration of the newly-formed drainage divide provides a new perspective for identifying the reorganization of the river network. Here, we employ numerical modeling to reproduce the characteristic phenomena of drainage-divide migration following capture events and analyze the effects of different parameters on the migration rate. We find that (1) the migration of newly-formed drainage divides can last for tens of millions of years, with the migration rate decreasing exponentially over time; (2) larger captured area, higher uplift rate, and lower erosional coefficient, all of which cause a higher cross-divide difference in steady-state elevation, will cause higher migration rate of the newly-formed drainage divide. This insight was further applied to the Dadu-Anning and Yarlung-Yigong capture events. We predict the present Dadu-Anning drainage divide would further migrate ~65–92 km southward to reach a steady state in tens of millions of years. The Yarlung-Yigong capture event occurred in the early-middle

Cenozoic, which implies that the late-Cenozoic increased exhumation rate is not related to the capture event.

Plain Language Summary

A capture event will lead to the formation of a new drainage divide between the capture point and the beheaded river. Then, the newly-formed drainage divide will migrate towards the beheaded river, a process called river-channel reversal. In this study, we used numerical modeling and natural examples to explore how a newly-formed drainage divide migrate after a river capture event. We find that the migration of newly-formed drainage divides can last for tens of millions of years, and the migration rate decreases exponentially over time. In addition, a larger captured area, higher uplift rate, or lower erosional coefficient can enhance the migration of the newly-formed drainage divide. We further applied our modeling to two natural examples. Our results show that the present Dadu-Anning divide is moving south and this process would last for tens of millions of years. The Parlung River has reversed its flow direction for over 200 km and reached a new steady state, which means an early formation of the modern Yarlung River, rather than the hypothetical Quaternary capture event of the Parlung River.

1 Introduction

The landscape equilibrium state can be upset by tectonic and/or climatic disturbances, as they alter the steady-state elevation of river channels (Whipple, 2001). When two river channels sharing a drainage divide have different steady-state elevations at their channel heads, the drainage divide will migrate toward the victim side with a higher steady-state elevation (Willett et al., 2014). The divide migration process will simultaneously decrease and increase the steady-state elevation of the victim and aggressor side, respectively, until the cross-divide difference is eliminated (Willett et al., 2014). The divide then reaches a new steady state and adapts to the new tectonic and climatic environment (He et al., 2021; Shi et al., 2021; Zhou et al., 2022a).

Contrary to continuous divide migration, discrete river capture events make a substantial adjustment in river network topology around the capture point (Morisawa, 1989; Bishop, 1995; Clark et al., 2004; Prince et al., 2011; Yanites et al., 2013; Lave, 2015; Stokes et al., 2018; Yang et al., 2020), and thus can rapidly change the steady-state elevation on both sides of the newly-formed drainage divide (Bishop, 1995; Goren et al., 2014; Willett et al., 2014; Shelef and Goren, 2021). As river capture events impact the evolution of the landscape, ecosystem, and even human civilizations (Winemiller et al., 2008; Willis et al., 2010; Hoorn et al., 2010; Xing et al., 2017), how and when they occurred is one of the major concerns for earth scientists (e.g., Clark et al., 2004; Fan et al., 2018; Yang et al., 2020). However, most capture events in case study remain controversial on their detailed processes and

occurring time (Clark et al., 2004; Cina et al., 2009; Lang and Huntington, 2014; King et al., 2016; Gourbet et al., 2017; Govin et al., 2018; Zhang et al., 2019; Zhao et al., 2021a, b).

Past river capture events could be inferred from barbed tributaries, wind gaps, abandoned river channels, paleocurrent direction, and provenance analysis (Bishop, 1995; Clark et al., 2004; Brocard et al., 2011; Zhang et al., 2012; Bracciali et al., 2015; Chen et al., 2017; Fan et al., 2018, 2021; Harel et al., 2019; Xie et al., 2020; Yang et al., 2021; Zhao et al., 2021a, b). However, to obtain the exact time of dating the capture event is more challenging based upon these methods. This is partially because only the river relict sediments before the capture event can record the paleocurrent direction and provide a constraint on the capture event timing. A capture event usually occurred several or even tens of millions of years ago. It is not easy to find the paleochannel sediments on the main trunk of the beheaded, or the reversal and captor rivers (Clark et al., 2004; Fan et al., 2010, 2018; Wei et al., 2016), even though the sediments usually only provide an upper or lower limit to the capture time.

One way to study the river capture process, circumventing the caveats in the conventional, sediment-based techniques, is via the analysis of drainage divides. Immediately after a capture event, the steady-state elevation of the captor river is much lower than that of the beheaded river, which can cause a new and greater disequilibrium. Then, the newly-formed drainage divide will migrate from the capture point towards the beheaded-river side, which results in a small, but significant phenomenon called *river-channel reversal* (Clark et al., 2004; Clift et al., 2006; Harel

et al., 2019; Yang et al., 2020; Shelef and Goren, 2021; Zeng and Tan, 2023). Therefore, the location and the stability of drainage divides, especially the newly-formed drainage divide between the reversal and the beheaded river channels, could provide new and independent constraints on the processes and time scales of the capture event.

In this study, we first use numerical modeling to explore the dynamics of river capture events and analyze the effects of captured area, uplift rate, and erosional coefficient on the migration rate of the newly-formed drainage divide. Then, we present two natural cases with significant river capture events, the Dadu-Anning in eastern Tibet and the Yarlung-Yigong in the eastern Himalayan syntaxis region to show how the modeling results are used to constrain the occurring time of capture events.

2 Background

To frame our analysis, we first make a conceptual overview of the river capture event. We then summarize analytical models of steady-state elevation at the channel heads. In addition, we briefly review the background on the Dadu-Anning and Yarlung-Yigong capture events, which are two typical natural cases of river capture on the Tibetan Plateau.

2.1 River capture event

River capture is a more common natural process with the interception of a river by an adjacent river as mountainous landscapes evolve (Bishop, 1995). So far, most

identified river captures occurred between two tributaries with relatively small drainage areas (usually several to hundreds of square kilometers), accompanied by wind-gap migration (Shelef and Goren, 2021). This process is termed ***tributary shift*** here (Figs. 1B). As the divide migrates across these trunk-tributary confluences, the ongoing tributary shift towards the aggressor side causes slight fluctuations in the cross-divide difference in steady-state elevation (Fig. 1C).

On the other hand, a more severe scenario exists, in which a river captures a vast area (such as thousands of square kilometers or greater) all at once by cutting the trunk of the other river. Such a catastrophic process is called ***capture event***, and is usually regarded as the landmark of river network reorganization (Figs. 1D-E). A capture event reduces the steady-state elevation of the captor river by increasing the upstream area and raises the steady-state elevation of the beheaded river by decreasing the upstream area (Willett et al., 2014; Yang et al., 2015; Whipple et al., 2017). Therefore, a capture event makes a significant cross-divide steady-state elevation contrast (Fig. 1F). In this study, we focus primarily on the capture events.

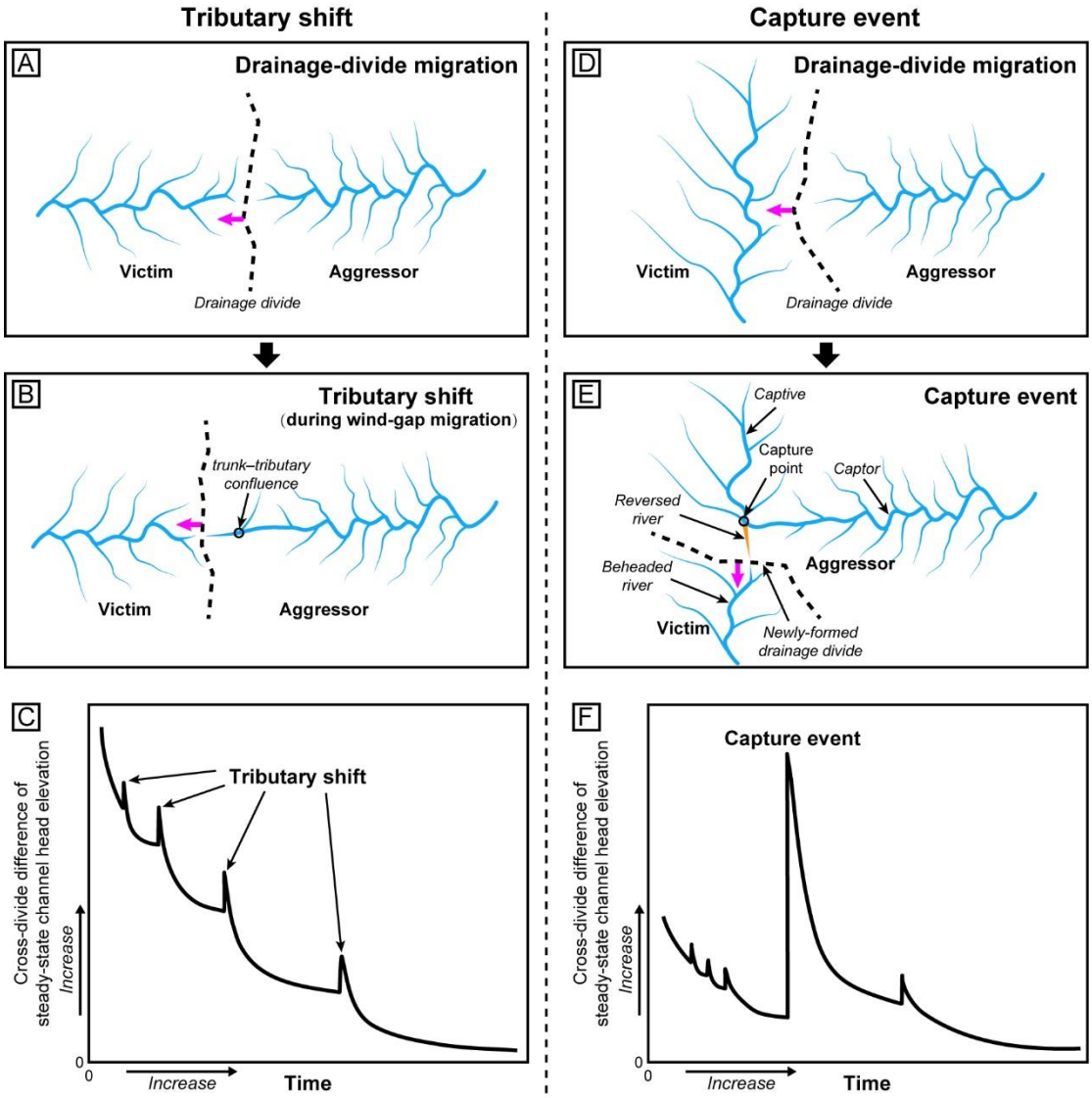

Fig. 1 Schematic illustration of tributary shift (A, B, C) and capture event (D, E, F). (A-B) A typical drainage-divide migration process with gradual shifts between tributaries. (C) The change of the cross-divide difference of steady-state channel-head elevation over time during the tributary shift process. The tributary shift can cause fluctuations in the cross-divide difference in steady-state elevation. (D-E) Illustrations of a significant drainage system reorganization after a capture event. Note the sudden, remarkable change in the river network. (F) The change of the cross-divide difference in steady-state channel-head elevation over time during the capture event. The capture event significantly increases the cross-divide difference of steady-state elevation.

2.2 Steady-state elevation and steady-state channel profile

Steady-state elevation is a theoretical value for which erosion would balance rock uplift (Whipple, 2001). It can be estimated from the model for river incision into bedrock (Whipple, 2001; Willett et al., 2014). According to the detachment-limited stream power model (Howard and Kerby, 1983), the erosion rate (E) is usually expressed as the following:

$$E = KA^m S^n \tag{2}$$

where K is the erosion coefficient, S is the channel gradient, A is the upstream area, and m and n are the area and slope exponents, respectively. At a steady state ($E = U$, U is uplift rate), Eq. (2) can be solved for the following expression (Kirby and Whipple, 2001):

$$S = \left(\frac{U}{K}\right)^{\frac{1}{n}} A^{\frac{-m}{n}} \tag{3}$$

The steady-state solution of a river channel profile (z) can be derived from integrating the channel distance (x):

$$z(x) = z_b + \int_{x_b}^{x} \left(\frac{U}{K}\right)^{\frac{1}{n}} A(x)^{\frac{-m}{n}}\, dx \tag{4}$$

where z_b is the elevation at the river base point. Parameter χ was introduced as an integral function of position in the river channel (Perron and Royden, 2013):

$$\chi = \int_{x_b}^{x} \left(\frac{A_0}{A(x)}\right)^{\frac{m}{n}} dx \tag{5}$$

where A_0 is an arbitrary scaling area to make the integrand dimensionless. Then, the steady-state solution of a river channel profile (z) can be expressed as:

$$z(x) = z_b + \left(\frac{U}{K}\right)^{\frac{1}{n}} (A_0)^{-\frac{m}{n}} \chi \tag{6}$$

2.3 Background on the Dadu-Anning capture event

The Dadu River, located in the eastern Tibetan Plateau, is a major tributary of the Yangtze River (Figs. 2A-B). It flows >600 km southwards from the Songpan-Ganze Terrane, and then makes an abrupt (~90°) loop at the town of Shimian, turning eastward into the Sichuan Basin. To the south of this river bend, a low and wide pass (wind gap) separates the Dadu River from the south-flowing Anning River. The Anning River drains a broad alluvial valley and finally converges with the Yangtze River (Fig. 2A). On the χ-plot (Fig. 2C), the Dadu River shows a high channel steepness in the middle reaches and less steep profiles in its upper and lower reaches, while the Anning River shows a gentle upper reach, and becomes steeper in its lower reach.

This river network pattern is suggested as a consequence of a capture event between the Dadu and Anning Rivers, based on the topography map, the existence of the wind gap, and fluvial sediments preserved within it (Clark et al., 2004; Yang et al., 2020; Zheng et al., 2023). The paleo-Dadu-Anning River originally flowed southward, and then was captured by an east-flowing paleo-Dadu River (Fig. 2B). The capture event formed the present Dadu River and beheaded the Anning River ("Anning" means quiet in Chinese). The newly-formed Dadu-Anning drainage divide was located close to the capture point (Shimian) and started to migrate southward (Fig. 2B). Yang et al. (2020) assigned this capture event at ~2.4 Ma based on provenance analysis, thermochronometry, topographic analysis, and numerical modeling.

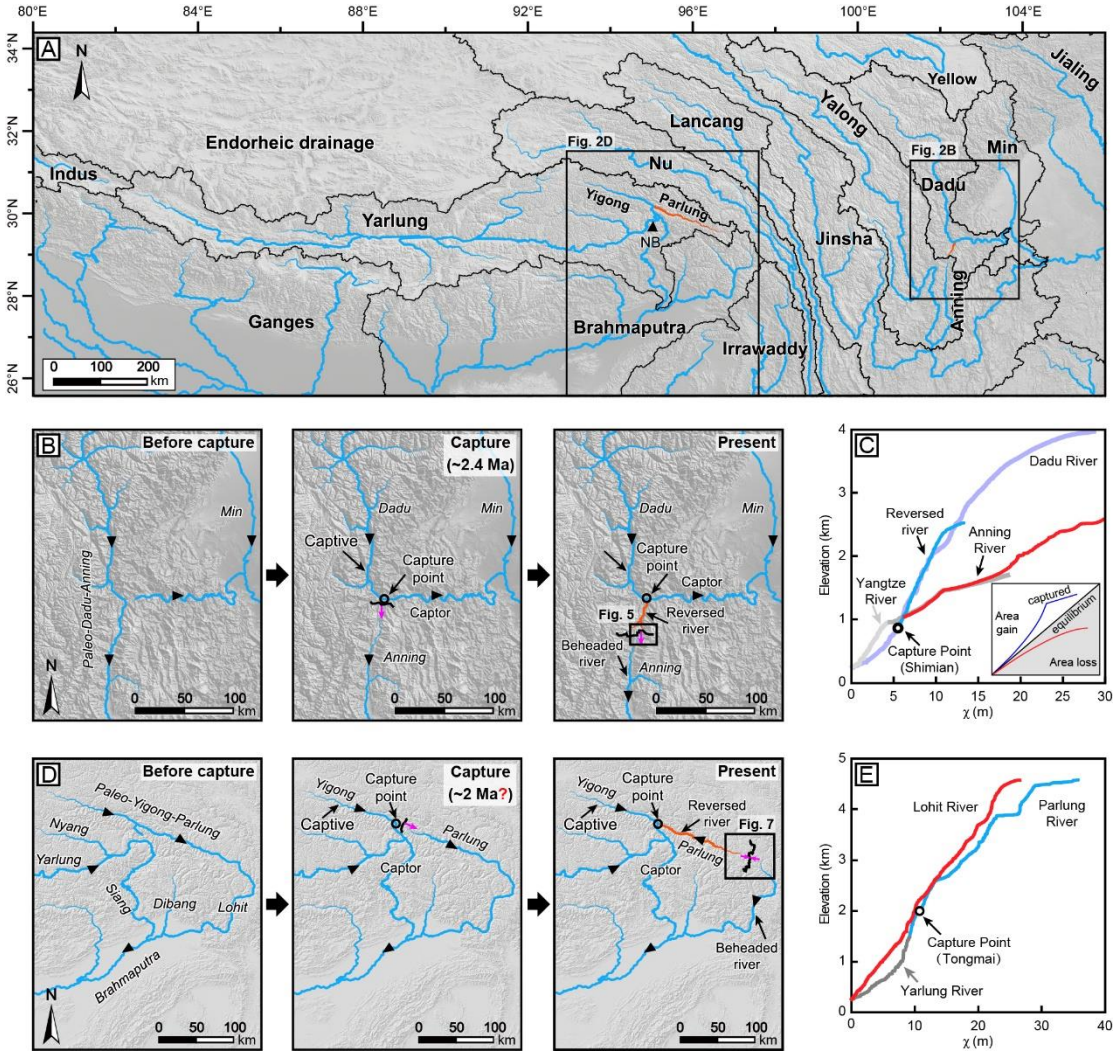

Fig. 2 (A) Overview of the major rivers and drainage basins in the Tibetan Plateau and surrounding region. (B) Illustration of the Dadu-Anning capture event. (C) χ-plots for the Dadu and Anning Rivers. (D) Illustration of the Yarlung-Parlung capture event. (E) χ-plots for the Parlung and Lohit Rivers.

2.4 Background on the Yarlung-Yigong capture event

In the eastern Himalayan orogenic belt, two major rivers, the southeast-flowing Yigong and northwest-flowing Parlung Rivers, incised the Namche Barwa massif and connected with the Siang River through the Tsangpo Gorge (Fig. 2A). After the confluence of the Siang, Dibang and Lohit Rivers, it becomes the Brahmaputra River. Along the Parlung River, all the barbed tributaries, wind gaps, and the low drainage

divide indicated that it has experienced river capture and reversal (Burchfiel et al., 2000; Clark et al., 2004; Seward and Burg, 2008; King et al., 2016; Yang et al., 2021).

Two end-member models have been proposed to explain the complex drainage pattern. Some authors suggested that the Yarlung River once flowed east into the Irrawaddy River through the Parlung River, which was sequentially captured by headward erosion of the Siang-Brahmaputra (Burchfiel et al., 2000; Clark et al., 2004; Robinson et al., 2014). Others postulated a paleo-Yigong-Parlung-Lohit River, with the capture of an antecedent Yarlung-Siang-Brahmaputra River (Seward and Burg, 2008; Lang and Huntington, 2014; Govin et al., 2018). Regardless of the method of capture, the reversal of the Parlung River first occurs at the present Yigong-Parlung confluence (the town of Tongmai), and then the newly-formed drainage divide moves eastward to its current position (Fig. 2C). The headwaters of the Parlung River are separated from the Lohit River by the Parlung-Lohit drainage divide.

3 Numerical modeling on landscape evolution

To explore the dynamics of river capture event and its control factors, we performed 10 numerical experiments using the TopoToolbox Landscape Evolution Model (Campforts et al., 2017). In addition, we further analyzed the effects of captured area, uplift rate, and erosional coefficient on the location and migration rate of the newly-formed drainage divide.

3.1 Reference Model

We first conduct a landscape evolution modeling to reproduce the evolution of the newly-formed drainage divide migration after a river capture event. The reference model (Fig. 3) extends 200 km long in the E-W direction and 300 km wide in the N-S

direction, which is resolved by a spatial resolution of 100 m. The initial elevation is set as a constant elevation of 1000 m on the northern edge, whereas the elevation at the southern edge is fixed to 0 m. The uplift rate is uniform across the model domain (3 mm/yr) except for a narrow zone in the east-central part of the model (X = 140–200 km; Y = 179–180 km), in which an eastward decreasing gradient zone of uplift rate is assigned to simulate an originally east-flowing river. Other model parameters in the reference model are set as follows: erosional coefficient (K) is 2×10^{-6}/year; area exponent (m), 0.5; slope exponent (n), 1; hillslope diffusivity, 0.03 m^2/year; and drainage area threshold, 0.1 km^2. The model was run for over 30 Myr, with a time step of 0.5 Myr (Movie S1).

Figure 3 shows selected representative snapshots of the reference model. At the initial stage, the drainage system contains a major, south-flowing river and a local, east-flowing river on the asymmetrically uplifted slope (Fig. 3A). Subsequently, the east-flowing river captures the south-flowing rivers, generating a new segment of the drainage divide between the reversal and the beheaded channels at the capture point (Fig. 3B). Due to this capture event, the area gain for the captor rivers increases the headwater channel steepness, and in turn leads to a fast erosion rate. In contrast, the beheaded river loses the upstream area, leading to a corresponding decrease in channel steepness and erosion rate. The cross-divide difference in erosion rate further drives the newly-formed drainage divide to migrate southward (Figs. 3C-D). As the divide migrates, the reversal river channel is elongated and the beheaded river channel shrinks. This results in an overall increase in the channel gradient of the beheaded river drainage compared to the reversal river drainage, and thus the drainage-divide migration rate slows down over time (Figs. 3D-F) (Braun, 2017; Whipple et al., 2017; Shelef and Goren, 2021).

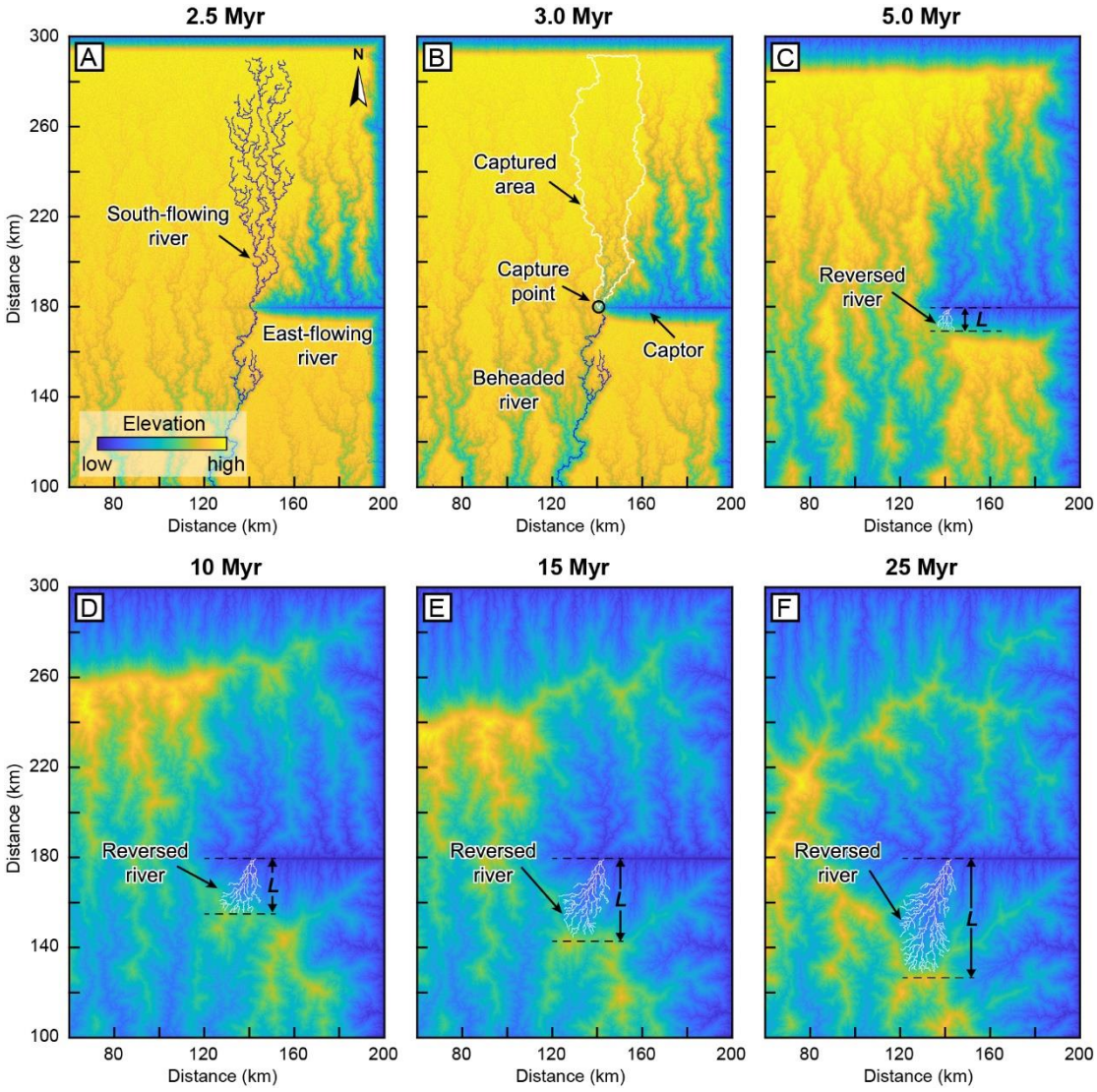

Fig. 3 Numerical landscape evolution model in response to a capture event. (A) The initial drainage system developed several south-flowing rivers and east-flowing rivers on the asymmetrically uplifted slope. (B) The originally south-flowing rivers are captured and turn to flow eastward. A new east-trending drainage divide was formed close to the capture point. (C-F) The newly-formed divide continues to migrate southward, resulting in an extension of the reversal channel. *L* represents the reversal distance, which refers to the vertical distance from the divide to the main trunk.

2.2 Effects of captured area

During the drainage-divide migration process, a river capture event

instantaneously alters the drainage area, that is, the drainage area is removed from the beheaded and added to the captor rivers. This process leads to a change in the steady-state elevation of channel heads across the newly-formed drainage divide (Fig. 1F), which further promotes the drainage divide to migrate towards the beheaded-river side (Willett et al., 2014; Whipple et al., 2017; Shelef and Goren, 2021; Ye et al., 2022). To delineate the effect of the captured area on the migration of the newly-formed drainage divide, we systematically varied the size of the captured area by proportionally enlarging the model domain (Figs. 4A-B; Supplementary Fig. S1). Other parameters remained the same as the reference model.

We first obtained the location of the newly-formed drainage divide at each moment (at a time step of 0.5 Myr). The distance between the drainage divide and the main trunk of the east-flowing river is called *river-channel reversal distance* (Fig. 3). We measured the reversal distance at 2 Myr intervals (Fig. 4A), and calculated the mean reversal rate (Fig. 4B). The mean reversal rate, V, can be estimated by the equation of $V = (L_2-L_1)/(t_2-t_1)$, where L_2 and L_1 are the reversal distances at two instants of t_2 and t_1, respectively. Here, we obtained the mean reversal rate every 2 Myr (i.e., t_2-t_1), except for a rate at the very beginning with the interval of 1 Myr.

Under different scenarios, the reversal rates exhibit similar trends, in which the value is the greatest in the early stage, exponentially decreases to half after ~2–3 Myr, and further declines smoothly towards zero in the following tens of millions of years (Fig. 4B). In addition, the reversal rate and reversal distance increase with increasing captured area. When the captured area is set to ~2,200 km^2, the reversal rate is ~7.5 mm/yr at the very beginning of the experiment (1 Myr) and then gradually slows down (Fig. 4B). In this case, the drainage divide has migrated ~60 km within ~20 Myr (Fig. 4A). When the captured area is increased to ~25,000 km^2, the reversal distance

288 is rapidly built up within the first ~8 Myr. The reversal rate in the early stage can
289 reach the peak value of ~18 mm/yr, which is greater than those in other models.

290 **2.3 Effects of uplift rate**

291 Drainage adjustment is strongly controlled by vertical tectonic movement
292 (Mitchell and Yanites, 2019; He et al., 2019; Shi et al., 2021; Ye et al., 2022), which
293 can be represented by various uplift rates in this circumstance. To test the effects of
294 tectonic on the migration rate of the newly-formed drainage divide, we assigned
295 various uplift rates of 1, 2, 3, and 4 mm/yr (Figs. 4C-D) for model runs. The size of
296 the captured area is constrained within a 10% error range with the reference model.
297 The landscape evolution processes (Supplementary Fig. S2) are comparable to the
298 reference model.

299 All the model results demonstrate that the newly-formed drainage divide after a
300 capture event migrates southward for more than 30 Myr (and still yet to reach a steady
301 state). The river-channel reversal rate decreases exponentially over time (Fig. 4D).
302 Moreover, the uplift rate facilitates the river-channel reversal. A higher uplift rate
303 results in a faster reversal rate and thus a longer reversal distance (Figs. 3C-D).

304 **2.4 Effects of erosional coefficient**

305 Lithology and climate can also affect the migration of drainage divides (e.g.,
306 Willett et al., 2001, 2014; Zondervan et al., 2020; Zhou et al., 2022a). Their effects are
307 implemented in the rock erosion coefficient in our models. A smaller erosion
308 coefficient means a stronger lithological unit or lower precipitation. Therefore, we
309 designed one group of models to examine the influence of the erosional coefficient
310 (Figs. 4E-F; Supplementary Fig. S3). The erosional coefficient is spatially uniform

and varies between 10^{-6}/year and 10^{-5}/year for different models, which is comparable to the values in the natural landscapes (e.g., Stock and Montgomery, 1999).

In this series of models, our results show that a low initial rock erosion coefficient is beneficial for the migration of the newly-formed drainage divide (Figs. 4E-F). A minor rock coefficient induces a lower erosion rate, which results in a flat, plateau-like surface across the south-flowing rivers in the early stage (Supplementary Fig. S3). This allows the captor rivers to drive the drainage divide to migrate rapidly southward, which results in a faster reversal rate (Fig. 4F). In contrast, a higher erosion coefficient accelerates river erosion but hinders divide migration and river-channel reversal.

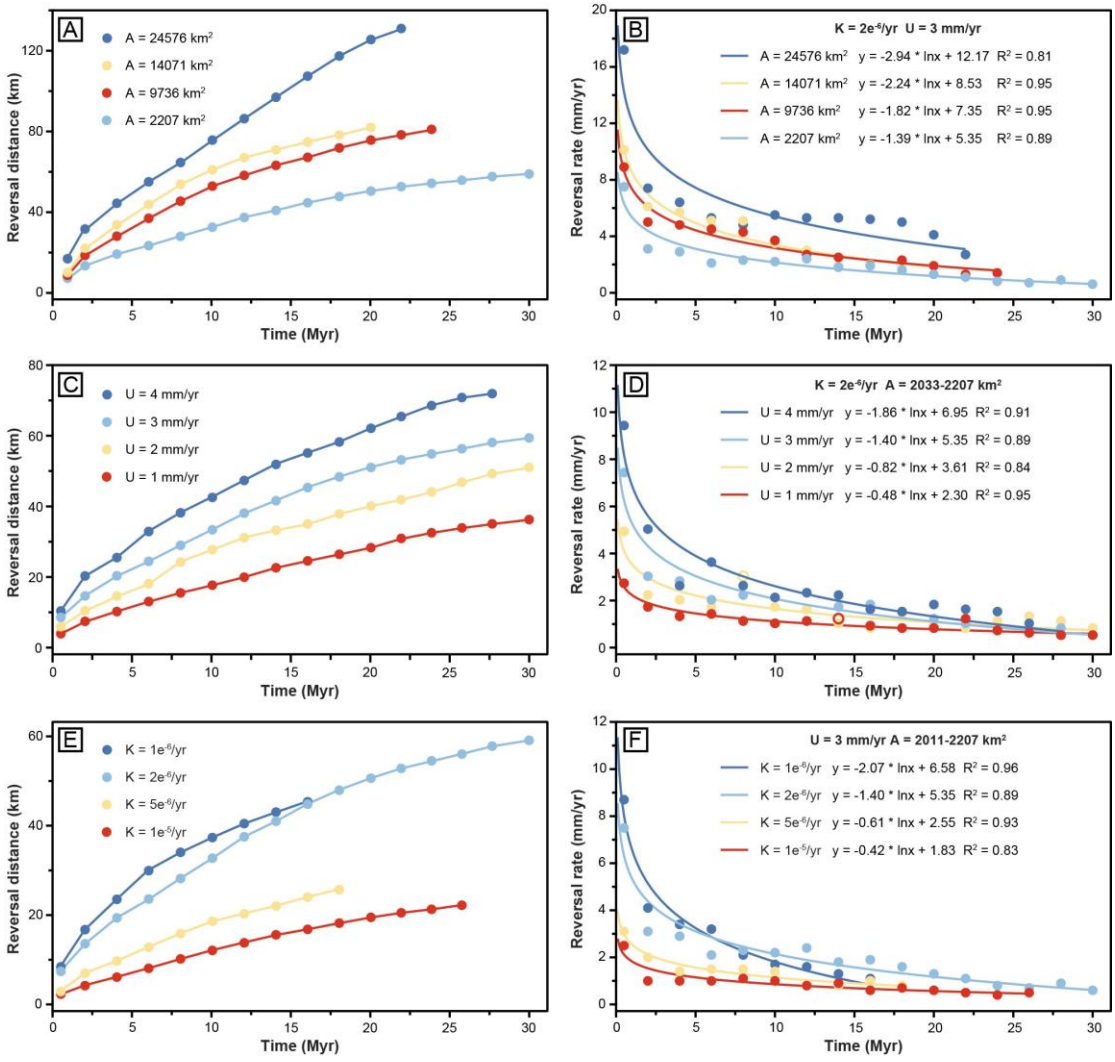

Fig. 4 The change of river-channel reversal distance and reversal rate over time in the models with different captured areas (A, B), uplift rates (C, D), and erosional efficiencies (E, F). The results show that the reversal rate exponentially decreases with time. The higher uplift rate, larger captured area, and lower erosional coefficient can lead to a faster reversal rate and thus longer reversal distance.

4 Application to natural landscapes

As above numerical modeling demonstrates, after a capture event, the newly-formed drainage divide between the reversal river and the beheaded river would migrate from the capture point towards the beheaded-river side until it reaches equilibrium or even undergoes an overturn. Therefore, in the case study, the stability and the location of the newly-formed drainage divides play a crucial role in revealing the river network reorganization process. Here, we evaluated the stability of the Dadu-Anning and Yarlung-Yigong drainage divides, respectively. With that, we predicate the future steady location of the Dadu-Anning drainage divide.

4.1 Dynamic Dadu-Anning drainage divide

Drainage-divide migration is essentially driven by the cross-divide difference in erosion rate (Willett et al., 2014; Forte and Whipple, 2018; He et al., 2021; Zhou et al., 2022a). Because the normalized channel steepness (k_{sn}) is positively and monotonically correlated with erosion rate (Kirby and Whipple, 2012), the comparisons on the k_{sn} value across the drainage divide have been used to evaluate the drainage-divide stability, assuming similar lithology and precipitation (Willett et al., 2014; Forte and Whipple, 2018; Chen et al., 2021). In particular, the k_{sn} value can be visualized by the slope of the χ-plots. Therefore, when comparing the top-most k_{sn} value (linear or quasi-linear χ-plots), a greater value (i.e., a steeper slope of χ-plot)

would force the drainage divide to migrate towards the other side (Zhou et al., 2022b).

We compared the cross-divide differences in topographic features, k_{sn}, and χ by the satellite imagery and χ map (Fig. 5). The Dadu drainage has steeper channels, higher k_{sn}, and lower χ values than those in the Anning drainage (Figs. 5A, B, D). Here, we show three paired tributaries through similar lithologies to compute the χ-plots. Among them, a pair of rivers close to the broad valley is characterized by a signature of drainage area gain by tributaries shift in the χ-plot (Fig. 5C) (Willett et al., 2014; Beeson et al., 2017). For other rivers, the upper reaches of the Dadu River have higher k_{sn} values (greater slopes) than those of the Anning River (Fig. 5C), indicating that the drainage divide is migrating southward. In summary, the above different methods show consistent results, where the Dadu-Anning drainage divide is moving south.

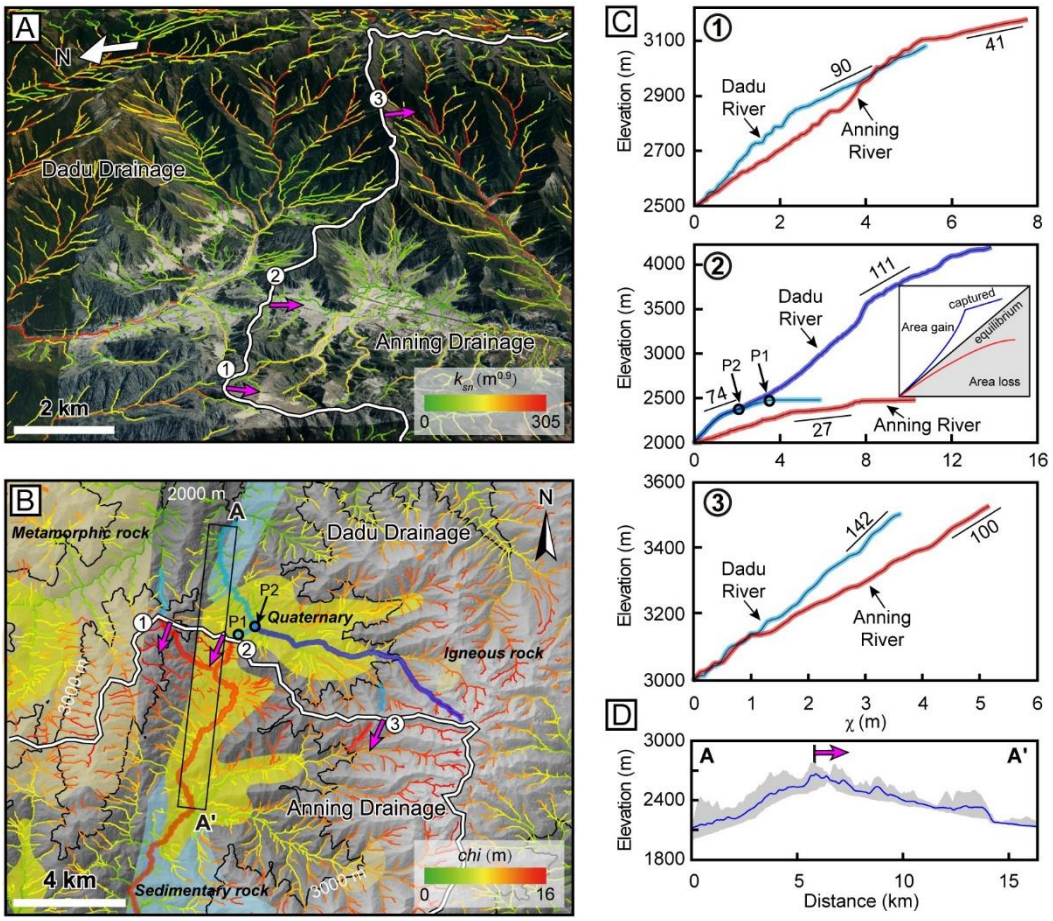

Fig. 5 Perspective views and χ map of channels for part of the Dadu-Anning drainage divides. The location is shown in Fig. 2B. (A) Perspective views of channels mapped with k_{sn}. The k_{sn} values in the Dadu drainage are generally larger than those in the Anning drainage. (B) Map of χ and geology. Arrows show the divide migration directions. P_1 and P_2 are the capture points. (C) χ-plots for three paired rivers across the divide. Numbers in the χ-plots are the average k_{sn} values. Rivers in red are the victims and those in blue are the aggressors. The results show that the Dadu-Anning divide is moving south. The reference drainage area is 10^5 m^2. (D) Swath profile A-A' of topography across the divide. Location of the swath is marked by the black rectangle in panel (B).

4.2 Future stable location of the Dadu-Anning drainage divide

To predicate the future steady location of the drainage divide, we calculated the cross-divide contrast index (*C*) (Zhou et al., 2022a). It amalgamates the across-divide differences in lithology, precipitation, channel height, and drainage-basin morphology by a quantitative theoretical relationship between the erosion coefficient (*K*), channel height (*H*), tortuosity coefficient (*T*), Hack's coefficient and exponent (*k* and *b*), area exponent (*m*), and slope exponent (*n*).

$$C = \left(\frac{K_\beta}{K_\alpha}\right)^{\frac{1}{n}}\left(\frac{H_\beta}{H_\alpha}\right)\left(\frac{T_\beta}{T_\alpha}\right)^{\frac{mb}{n}-1}\left(\frac{k_\beta}{k_\alpha}\right)^{\frac{m}{n}} \quad (1)$$

where subscripts α and β represent the two sides of the drainage divide. In this study, α is the northern side, and β is the southern side.

A pair of typical rivers close to the wind gap was selected (Fig. 6A). They flow into the main trunk of the Dadu and Yangtze Rivers, respectively. We measured the *H* and *T* at each side of the divide in ArcGIS software and determined the Hack's coefficient (k_α and k_β) and exponent (*b*) by fitting the drainage area and channel length (Fig. 6B) (Hack, 1957; Zhou et al., 2022a). Then, we calculated the *C* value combined with a uniform erosion coefficient (K_β/K_α =1). The detailed results are

shown in Supplementary Table S1. Accordingly, we plotted the relationship diagram between the normalized drainage divide location ($D_\beta/(D_\alpha + D_\beta)$) and uplift rate ratio (U_β/U_α) (Fig. 6C). With a wide range of the U_β/U_α (0.5–1), the $D_\beta/(D_\alpha + D_\beta)$ value is determined as 63.2%–53.5%. Based on the present normalized location of the Dadu-Anning divide (~86.5%), we predict that the drainage divide would continue to migrate southward for ~65–92 km. It is worth noting that there may be errors in this value due to the inhomogeneous lithology (Supplementary Fig. S4) along the river channel.

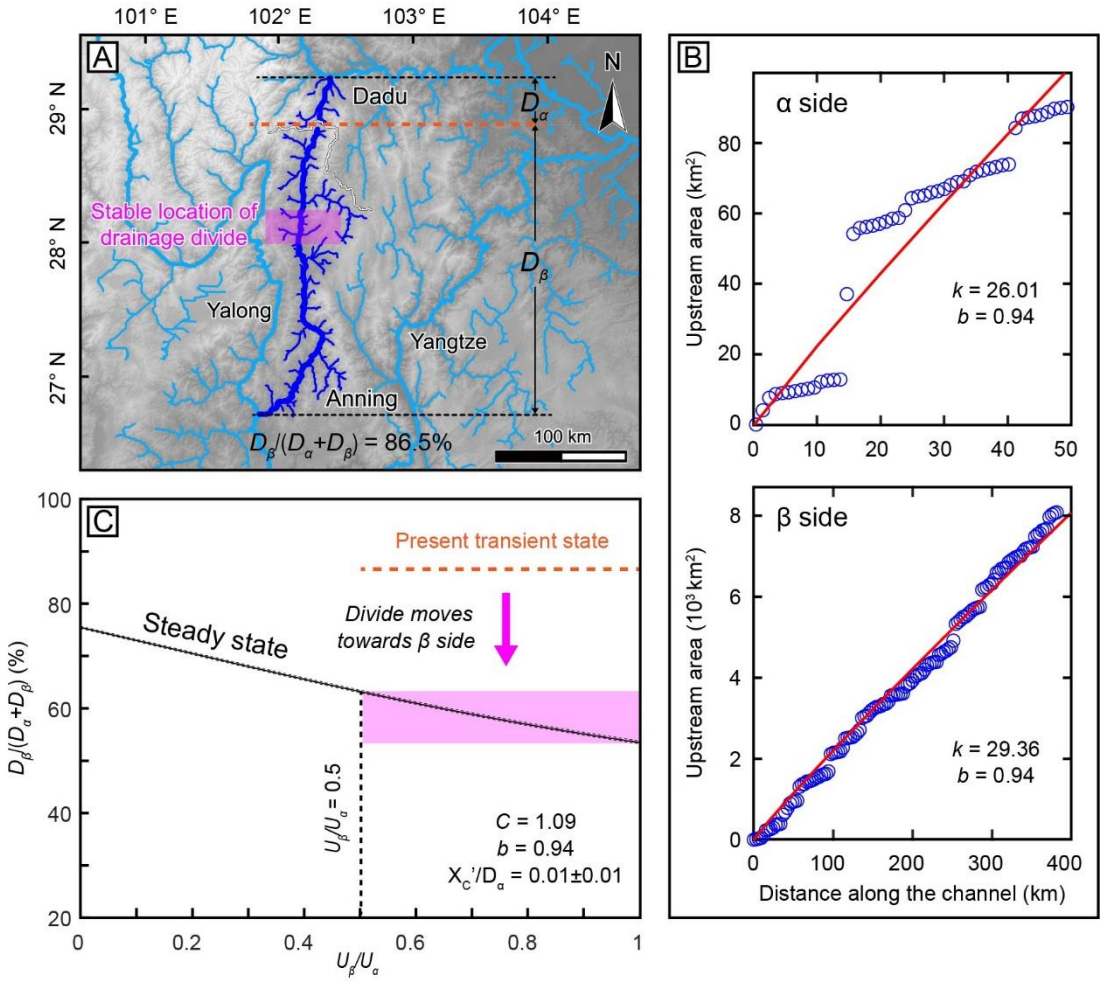

Fig. 6 Prediction for the steady location of the Dadu-Anning drainage divide. (A) Topography and drainage system. River segments highlighted in dark blue are measured and analyzed.

The burgundy area is the predicted steady location. (B) The Hack's coefficient and exponent (k and b). (C) The relationship diagram between the normalized drainage divide location ($D_\beta / (D_\alpha + D_\beta)$) and uplift rate ratio (U_β/U_α).

4.3 Stable Yarlung-Yigong drainage divide

To analyze the stability of the Parlung-Lohit drainage divide, we first compared the difference in k_{sn} value across the divide (Willett et al., 2014; Scherler and Schwanghart, 2020). Fig. 7A is the k_{sn} distribution pattern yield by the ArcGIS software. Along a 500-meter-wide swath, the k_{sn} values are comparable between two sides of the drainage divide (Fig. 7B). We also measured the top-most k_{sn} value of four paired rivers across the drainage divide. These rivers are distributed in four sections of the Parlung-Lohit drainage divide (the ab, bc, cd, and de sections), respectively. The χ-plot pairs show near-parallel profiles and thus approximately equal k_{sn} values (Fig. 7C). Therefore, the results show that the Parlung-Lohit drainage divide is stable.

In addition, we adopted the Gilbert metrics method (Forte and Whipple, 2018) to analyze the four segments along the drainage divide. The Gilbert metrics incorporate the cross-divide differences in mean headwater local relief, mean headwater hillslope gradient, and channel elevation at a reference drainage area (Whipple et al., 2017; Forte and Whipple, 2018). The drainage divide will migrate towards the side with a lower slope, lower relief, or higher elevation in an asymmetrical mountain. In this study, we used a reference drainage area of 10^5 m^2 to calculate the Gilbert metrics. According to the standardized analysis of drainage migration direction (Fig. 7D), four segments show that the current divide is at a stable state, which is consistent with the results from the χ-plots.

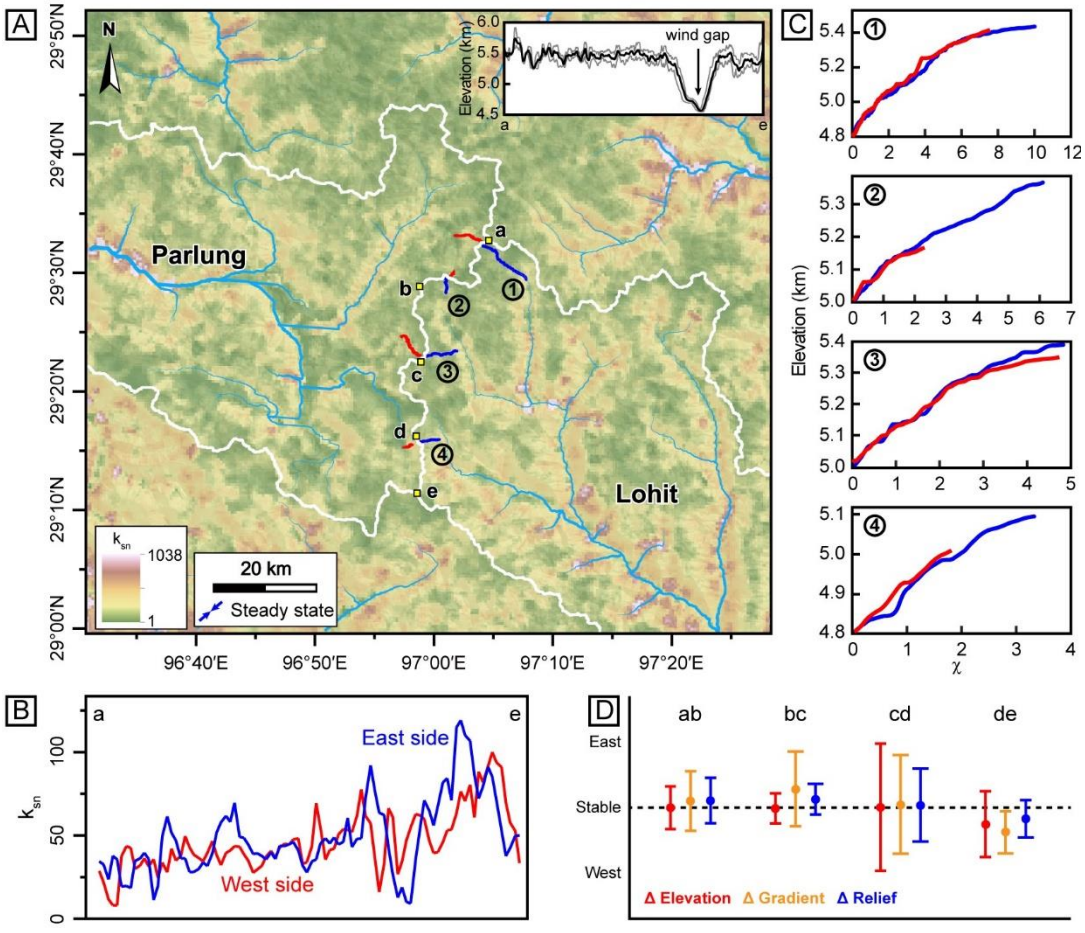

Fig. 7 (A) The k_{sn} map of the Yigong and Parlung drainages. See Fig. 2C for location. Insert figure is an elevation profile along the drainage divide (a-e), where the black arrows indicate the locations of the wind gaps. (B) Comparison of the k_{sn} values between the two sides of the Yigong-Parlung drainage divide along a 500-meter-wide swath. (C) χ-plots for four paired rivers across the divide. (D) Standardized delta plot for the four segments along the Yigong-Parlung drainage divide. The results are calculated by the DivideTools in TopoToolbox (Schwanghart and Scherler, 2014; Forte and Whipple, 2019). The different methods above show consistent results, where the Yigong-Parlung divide is steady.

5 Discussion

5.1 Effects of different parameters on divide migration following a capture event

A capture event can significantly adjust the river network topology, and thus

cause an abrupt change of steady-state elevations along river channels. Willett et al. (2014) suggested that the drainage divide will migrate towards the river basin with higher steady-state elevation at the channel head. In this way, the drainage-divide migration following a river capture event is closely related to the cross-divide difference in steady-state elevation at the channel heads.

Based on the quantitative relationships (Eqs. 5 and 6) of the steady-state elevation, we analyzed the effects of capture area, uplift rate, and erosional coefficient on drainage-divide migration. A sudden adjustment in drainage area instantaneously changes χ but not riverbed elevation (Willett et al., 2014; Whipple et al., 2017). In general, the channel head of the captor river has a lower steady-state elevation than that at the future capture point, which drives the divide migration and eventually leads to the capture event. However, for brevity, we assume that the channel head of the captor river has a similar steady-state elevation to that at the future capture point before the capture event. That is to say, the pre-existing cross-divide difference of steady-state elevation before the capture event was not taken into account. After a capture event, the beheaded river loses lots of upstream areas, which causes the increase of χ and then yields a higher steady-state elevation (Fig. 8A) (Willett et al., 2014). Similarly, the decrease in χ with area gain for captor rivers leads to a lower steady-state elevation. Therefore, the capture event will substantially increase the contrast of the steady-state elevation across the newly-formed drainage divide. A larger captured area can theoretically expand this contrast (Fig. 8A). The numerical modeling results reveal that a larger captured area will drive faster drainage-divide

migration when other conditions are the same (Figs. 4A-B).

In the case of increasing uplift rate or decreasing erosional coefficient (with other conditions being unchanged), the captor and beheaded rivers experience a uniform increase in riverbed elevation, and the steady state profile ($E = U$) becomes steeper accordingly (Fig. 8B). A capture event (with the same captured area) will increase the cross-divide difference in the steady-state elevation at the channel heads (Fig. 8B). Higher uplift rate or lower erosional coefficient will drive the higher cross-divide difference in the steady-state elevation at the channel heads, and further enhance the rate of drainage-divide migration, which is consistent with the result in the numerical modeling (Figs. 4C-F).

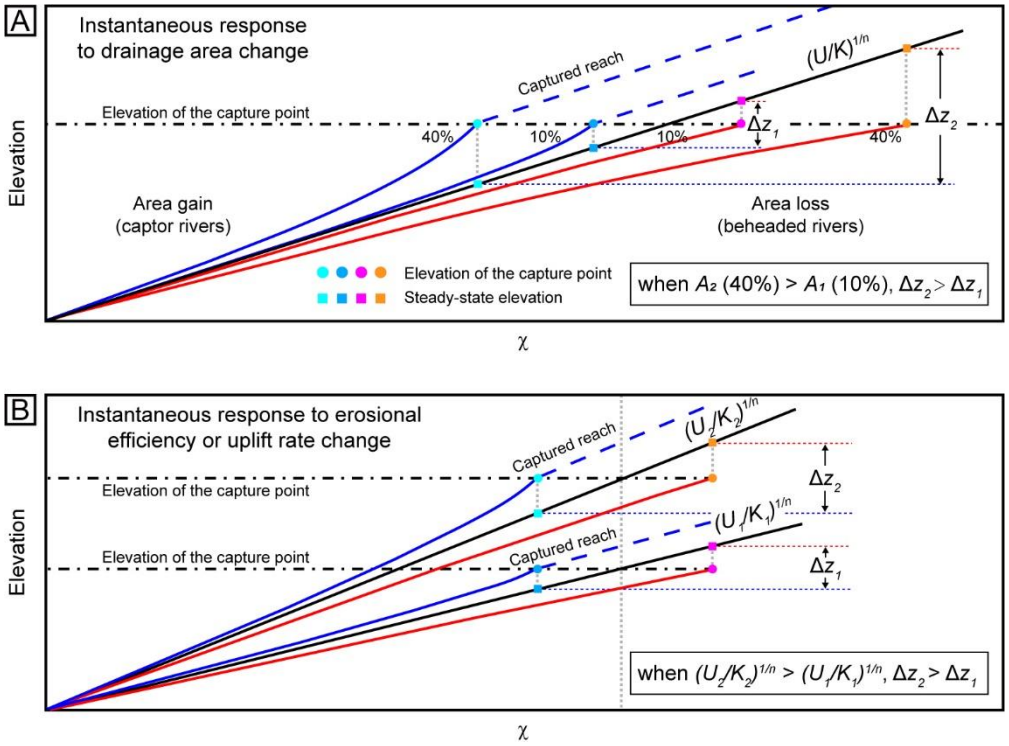

Fig. 8 (A) Schematic illustration of river profile response to drainage area change. A capture event will decrease the steady-state elevation for captor rivers gaining upstream area and increase the steady-state elevation for the beheaded rivers losing upstream area. A larger

captured area can expand this contrast, and accelerate the divide migration. (B) Schematic illustration of river profile response to uplift rate and erosion coefficient change. Increasing the uplift rate or decreasing the erosional coefficient can increase a cross-divide steady-state elevation contrast. Δz represents the cross-divide difference in steady-state channel-head elevation.

In summary, the larger captured area, higher uplift rate, or lower erosional coefficient can cause higher cross-divide differences in steady-state elevation of the channel heads, which facilitates the migration of the newly-formed drainage divide following a capture event.

5.2 The timescale of the Dadu-Anning drainage divide achieving a steady state

The modern Dadu and Anning Rivers have experienced an Early Pleistocene (~2.4 Ma) capture event (Yang et al., 2020), where the upper course of the original southward-flowing paleo-Dadu-Anning River was captured by an east-flowing paleo-Dadu River (Fig. 2B). The newly-formed Dadu-Anning drainage divide has migrated southward for ~40 km from the capture point (Fig. 2B). The result corresponds to a mean river-channel reversal rate of ~16.7 mm/yr from the moment of the capture event to present.

Our results show that the Dadu-Anning drainage divide is moving south at present, and would further migrate ~65–92 km southward to reach a steady state (Fig. 6). It implies that the present Dadu-Anning drainage divide has only migrated less than half of the total migration (from the capture point to the final steady state of the drainage divide). Meanwhile, our numerical modeling indicates that the reversal rate rapidly decreases to half of the original value after ~2–3 Myr (Fig. 4). If, thereafter,

494 the channel reversal rate decreases to ~8.4 mm/yr, the Dadu-Anning divide would
495 take another ~11–8 Ma to reach a steady state. Taking into account that the reversal
496 rate further decreases with time in the future (Fig. 4), this timescale of the
497 drainage-divide migration to achieve an equilibrium will be significantly extended.
498 Therefore, we conclude that the Dadu-Anning drainage divide would reach a steady
499 state in tens of millions of years, which is consistent with that in the numerical
500 modeling in this study (Figs. 3, 4) and those in previous studies (Shelef and Goren,
501 2021; Ye et al., 2022).

502 **5.3 Constraints on the timing of the Yarlung-Yigong capture event**

503 The current Parlung River has reversed its direction and flows northwest for
504 more than 200 km. However, the timing of this capture event is a subject of
505 controversy. One proposed explanation is that the paleo-Yarlung-Parlung-Irrawaddy
506 River was captured by the Siang River, leading to the reversal of the Parlung River
507 (Clark et al., 2004). This capture event was constrained at ~10 Ma (Brookfield, 1998;
508 Robinson et al., 2014) or prior to ~4 Ma (Zeitler et al., 2001; Clark et al., 2004).
509 Alternatively, recent studies have argued that the headward cutting
510 Yarlung-Siang-Brahmaputra captured the Parlung River in the Quaternary, as
511 indicated by thermochronological data (Seward and Burg, 2008; Zeitler et al., 2014;
512 King et al., 2016; Yang et al., 2021) and provenance analysis (Lang and Huntington,
513 2014; Govin et al., 2018).

514 Our observations, based on the stability analysis and numerical modeling,
515 provide a new perspective on this debate. We find that the Parlung-Lohit drainage
516 divide is stable at present (Fig. 7), which implies that it has migrated ~200 km from
517 the capture point towards the southeast and reached a steady state. According to the

518 modeling results in this study (Fig. 4) and those in previous studies (Willett et al.,
519 2014; Beeson et al., 2017; Whipple et al., 2017; Shelef and Goren, 2021), the
520 river-channel reversal process could continue for tens of million years. Therefore, a
521 Quaternary capture event would not be sufficient for a newly-formed drainage divide
522 to achieve an equilibrium position. This idea can also be supported by the case of the
523 Dadu-Anning capture, where the divide only migrated ~40 km to the south within
524 ~2.4 Ma (Yang et al., 2020) and is currently moving south with a largely decreased
525 migration rate but a longer remaining distance (~65–92 km) (Fig. 5). Furthermore, the
526 area of the Yigong Drainage (~13000 km^2) captured by Yarlung-Brahmaputra or the
527 Siang Rivers is much smaller than the captured area (~64000 km^2) by the paleo-Dadu
528 River, making it even more unlikely that the time of the Yarlung-Yigong capture event
529 is earlier than that of the Dadu-Anning capture event. Therefore, the results in this
530 study support that the Yarlung-Yigong capture event occurred in the early-middle
531 Cenozoic.

532 In the Namche Barwa syntaxis, bedrock and detrital thermochronology data
533 revealed an acceleration of exhumation rates along the lower reaches of the Yigong
534 and Parlung Rivers in the past 1–2 Ma (Seward and Burg, 2008; King et al., 2016;
535 Bracciali et al., 2016; Yang et al., 2018, 2021; Govin et al., 2020). This rapid
536 exhumation was suggested as a signal for the capture event of the Parlung River.
537 However, our results tend to favor an early formation of the current Yarlung River
538 pattern, rather than the hypothesis of Quaternary capture. It implies that the late
539 Cenozoic increased exhumation rate is not driven by the capture event. In this case,
540 the increased exhumation in the northern part may be attributed to a northward
541 expansion of the syntaxis (Seward and Burg, 2008; Wang et al., 2014; King et al.,
542 2016; Yang et al., 2018). In addition, spatiotemporal variations of precipitation may

play a role in the rapid exhumation. The strengthened precipitation in the lower reaches of the Yarlung River can reduce the elevation of the riverbed, which can accelerate the exhumation in Namche Barwa syntaxis (Zeitler et al., 2001; Yu et al., 2011).

This study demonstrates the process of drainage-divide migration following a river capture event, which helps to understand the evolution of rivers and offers an opportunity to constrain the time of capture events from a new perspective. However, there are still some limitations in this study. Our modeling does not account for the presence of unconsolidated sediments, which are commonly associated with river capture events (Clark et al., 2004; Zeng and Tan, 2023). This may result in an underestimation of the simulated reversal rate. In addition, the tributaries and their avulsions on drainage-divide migration can play a critical role in the reversal rate and extent (Shelef and Goren, 2021), but are not considered in our models. How these two factors influence the migration of the newly-formed drainage divide following a river capture event, however, is beyond the scope of this study, and deserves rigorous analysis in future studies.

6 Conclusions

(1) Numerical modeling results show that the newly-formed drainage divide following a river capture event will migrate lasting for tens of millions of years, with the migration rate decreasing exponentially over time. A larger captured area, higher uplift rate, or lower erosional coefficient can increase cross-divide steady-state elevation contrast, and further enhance the rate of drainage-divide migration.

(2) The present Dadu-Anning divide is moving south, which would last for tens of millions of years and further migrate ~65–92 km southward to reach a steady state.

(3) The Parlung River has reversed its flow direction for over 200 km after the Yarlung-Yigong capture event, and the river network has reached a new steady state. Our findings support an early formation of the modern Yarlung River, rather than the hypothesis of the Quaternary capture event of the Parlung River. This implies that the late Cenozoic increased exhumation rate was not driven by the Yarlung-Yigong capture event.

Acknowledgments

This study is supported by the Fundamental Research Funds for the State Key Laboratory of Earthquake Dynamics (LED2022A04 and LED2021A02), the CAS Pioneer Hundred Talents Program (E2K2010010), the National Natural Science Foundation of China (42202249).

Data Availability Statement

The topography data is from https://search.asf.alaska.edu/. The precipitation data are downloaded from http://worldclim.org. Procedures to perform the calculations are implemented through the Topographic Analysis Kit (Forte and Whipple, 2019) and DivideTools (Forte and Whipple, 2018) based on TopoToolbox (Schwanghart and Scherler, 2014).

References

Beeson, H. W., Mccoy, S. W., & Keen-Zebert, A. (2017). Geometric disequilibrium of river basins produces long-lived transient landscapes. Earth and Planetary Science Letters, 475, 34–43. https://doi.org/10.1016/j.epsl.2017.07.010

Bishop, P. (1995). Drainage rearrangement by river capture, beheading and diversion. Progress in Physical Geography, 19, 449–473. https://doi.org/10.1177/030913339501900402

Bracciali, L., Najman, Y., Parrish, R. R., Akhter, S. H. & Millar, I. (2015). The Brahmaputra tale of tectonics and erosion: Early Miocene river capture in the Eastern Himalaya. Earth and Planetary Science Letters, 415, 25–37. https://doi.org/10.1016/j.epsl.2015.01.022

Bracciali, L., Parrish, R. R., Najman, Y., Smye, A., Carter, A., & Wijbrans, J. R. (2016). Plio-Pleistocene exhumation of the eastern Himalayan syntaxis and its domal 'pop-up'. Earth-science Reviews, 160, 350–385. https://doi.org/10.1016/j.earscirev.2016.07.010

Braun, J. (2017). A review of numerical modeling studies of passive margin escarpments leading to a new analytical expression for the rate of escarpment migration velocity. Gondwana Research, 53, 209–224. https://doi.org/10.1016/j.gr.2017.04.012

Brocard, G., Teyssier, C., Dunlap, W. J., Authemayou, C., Simon-Labric, T., Cacao-Chiquín, E. N., et al. (2011). Reorganization of a deeply incised drainage: Role of deformation, sedimentation and groundwater flow. Basin Research, 23(6), 631–651. https://doi.org/10.1111/j.1365-2117.2011.00510.x

Brookfield, M. (1998). The evolution of the great river systems of southern Asia during the Cenozoic India-Asia collision: rivers draining southwards. Geomorphology, 22, 285–312. https://doi.org/10.1016/S0169-555X(97)00082-2

Burchfiel, B. C., Clark, M. K., Wang, E., Chen, Z., Liu, Y., & Pan, G. (2000). Tectonic framework of the Namche Barwa region, eastern Himalayan syntaxis, SE Tibet. Geological Society of America Special Paper, 32(7), A–33.

Campforts, B., Schwanghart, W., & Govers, G. (2017). Accurate simulation of transient landscape evolution by eliminating numerical diffusion: the TTLEM 1.0 model. Earth Surface Dynamics, 5(1), 47–66. https://doi.org/10.5194/esurf-5-47-2017

Chen, C., Willett, S. D., Christl, M., & Shyu, J. B. H. (2021). Drainage basin dynamics during the transition from early to mature orogeny in Southern Taiwan. Earth and Planetary Science Letters, 562, 116874. https://doi.org/10.1016/j.epsl.2021.116874

Chen, Y., Yan, M., Fang, X., Song, C., Zhang, W., Zan, J., et al. (2017). Detrital zircon U-Pb geochronological and sedimentological study of the Simao Basin, Yunnan: implications for

617 the Early Cenozoic evolution of the Red River. Earth and Planetary Science Letters, 476, 22–
618 33. https://doi.org/10.1016/j.epsl.2017.07.025
619 Cina, S. E., An, Y., Grove, M., Dubey, C. S., Shukla, D. P., Lovera, O. M., et al. (2009). Gangdese
620 arc detritus within the eastern Himalayan Neogene foreland basin: implications for the
621 Neogene evolution of the Yalu-Brahmaputra River system. Earth and Planetary Science
622 Letters, 285(1–2), 150–162. https://doi.org/10.1016/j.epsl.2009.06.005
623 Clark, M., Schoenbohm, L. M., Royden, L. H., Whipple, K. X., Burchfiel, B. C., Zhang, X., et al.
624 (2004). Surface uplift, tectonics, and erosion of eastern Tibet from large-scale drainage
625 patterns. Tectonics, 23(1), TC1006. https://doi.org/10.1029/2002TC001402
626 Clift, P.D., Blusztajn, J., & Anh Duc, N. (2006). Large-scale drainage capture and surface uplift in
627 eastern Tibet-SW China before 24 Ma inferred from sediments of the Hanoi Basin, Vietnam.
628 Geophysical Research Letters, 33, 19. http://dx.doi.org/10.1029/2006GL027772, L19403.
629 Fan, N. N., Chu, Z., Jiang, L., Hassan, M. A., Lamb, M. P., & Liu, X. (2018). Abrupt drainage
630 basin reorganization following a Pleistocene river capture. Nature Communication, 9, 1–6.
631 https://doi.org/10.1038/s41467-018-06238-6
632 Fan, N. N., Kong, P., Robl, J. C., Zhou, H. W., Wang, X. Y., Jin, Z. D., et al. (2021). Timing of
633 river capture in major Yangtze River tributaries: Insights from sediment provenance and
634 morphometric indices. Geomorphology, 392, 107915.
635 https://doi.org/10.1016/j.geomorph.2021.107915
636 Fan, N. N., Wu, B. & Liu, L. (2010). River avulsion by earthquake and the transition of ancient
637 Shu Civilization. Journal of Mountain Science, 28, 453–462. (in Chinese with an English
638 abstract).
639 Forte, A. M., & Whipple, K. X. (2018). Criteria and tools for determining drainage divide stability.
640 Earth and Planetary Science Letters, 493, 102–117. https://doi.org/10.1016/j.epsl.2018.04.026
641 Forte, A. M., & Whipple, K. X. (2019). Short communication: The Topographic Analysis Kit
642 (TAK) for TopoToolbox. Earth Surface Dynamics, 7, 87–95.
643 Goren, L., Fox, M., & Willett, S. D. (2014). Tectonics from fluvial topography using formal linear
644 inversion; theory and applications to the Inyo Mountains, California. Journal of Geophysical
645 Research: Earth Surface, 119, 1651–1681. https://doi.org/10.1002/2014JF003079

Gourbet, L., Leloup, P. H., Paquette, J.L., Sorrel, P., Maheo, G., Wang, G., et al. (2017). Reappraisal of the Jianchuan Cenozoic basin stratigraphy and its implications on the SE Tibetan plateau evolution. Tectonophysics, 700–701, 162–179. https://doi.org/10.1016/j.tecto.2017.02.007

Govin, G., Najman, Y., Copley, A., Millar, I., van der Beek, P., Huyghe, P., et al. (2020). Early onset and late acceleration of rapid exhumation in the Namche Barwa syntaxis, eastern Himalaya. Geology, 48(12), 1139–1143. https://doi.org/10.1130/G47720.1

Govin, G., Najman, Y., Dupont-Nivet, G., Millar, I., van der Beek, P., Huyghe, P., et al. (2018). The tectonics and paleo-drainage of the easternmost Himalaya (Arunachal Pradesh, India) recorded in the Siwalik rocks of the foreland basin. American Journal of Science, 318, 764–798. https://doi.org/10.2475/07.2018.02

Hack, J. T. (1957). Studies of longitudinal stream profiles in Virginia and Maryland. In: U.S. Geological Survey Professional Paper, pp. 45–97

Harel, E., Goren, L., Shelef, E., & Ginat, H. (2019). Drainage reversal toward cliffs induced by lateral lithologic differences. Geology, 47, 928–932. https://doi.org/10.1130/G46353.1

He, C. Q., Yang, C. J., Turowski, J. M., Rao, G., Roda-Boluda, D. C., & Yuan, X. P. (2021). Constraining tectonic uplift and advection from the main drainage divide of a mountain belt. Nature Communication, 12(1), 544. https://doi.org/10.1038/s41467-020-20748-2

He, C., Rao, G., Yang, R., Hu, J., Yao, Q., & Yang, C. J. (2019). Divide migration in response to asymmetric uplift: Insights from the Wula Shan horst, North China. Geomorphology, 339, 44–57. https://doi.org/10.1016/j.geomorph.2019.04.024.

Hoorn, C., Wesselingh, F. P., ter Steege, H., Bermudez, M. A., Mora, A., Sevink, J., et al. (2010). Amazonia through time: Andean uplift, climate change, landscape evolution, and biodiversity. Science, 330, 927–931. https://doi.org/10.1126/science.1194585

Howard, A.D., & Kerby, G., 1983. Channel changes in badlands. Geological Society of America Bulletin, 94(6), 739–752. https://doi.org/10.1130/0016-7606(1983)94<739:CCIB>2.0.CO;2

King, G. E., Herman, F., & Guralnik, B. (2016). Northward migration of the eastern Himalayan syntaxis revealed by OSL thermochronometry. Science, 353, 800–804. https://doi.org/10.1126/science.aaf2637

Kirby, E., & Whipple, K. (2001). Quantifying differential rock-uplift rates via stream profile analysis. Geology, 29(5), 415–418. https://doi.org/10.1130/0091-7613(2001)029<0415:QDRURV>2.0.CO;2.

Kirby, E., & Whipple, K. X. (2012). Expression of active tectonics in erosional landscapes. Journal of Structural Geology, 44, 54–75. https://doi.org/10.1016/j.jsg.2012.07.009

Lang, K. A., & Huntington, K. W. (2014). Antecedence of the Yarlung-Siang-Brahmaputra River, eastern Himalaya. Earth and Planetary Science Letters, 397, 145–158. https://doi.org/10.1016/j.epsl.2014.04.026

Lave, J. (2015). Landscape inversion by stream piracy. Nature, 520, 442–444.

Mitchell, N. A., & Yanites, B. J. (2019). Spatially variable increase in rock uplift in the northern US Cordillera recorded in the distribution of river knickpoints and incision depths. Journal of Geophysical Research: Earth Surface, 124(5), 1238-1260. https://doi.org/10.1029/2018JF004880

Morisawa, M. (1989). Rivers and valleys of Pennsylvania, revisited. Geomorphology, 2, 1–22.

Perron, J.T., & Royden, L. (2013). An integral approach to bedrock river profile analysis. Earth Surface Processes and Landforms, 38 (6), 570–576. https://doi.org/10.1002/esp.3302.

Prince, P. S., Spotila, J. A. & Henika, W. S. (2011). Stream capture as driver of transient landscape evolution in a tectonically quiescent setting. Geology, 39, 823–826. https://doi.org/10.1130/G32008.1

Robinson, R. A., Brezina, C. A., Parrish, R. R., Horstwood, M. S. A., Oo, N. W., Bird, M. I., et al. (2014). Large rivers and orogens: The evolution of the Yarlung Tsangpo-Irrawaddy system and the eastern Himalayan syntaxis. Gondwana Research, 26, 112–121. https://doi.org/10.1016/j.gr.2013.07.002

Scherler, D., & Schwanghart, W. (2020). Drainage divide networks – part 2: Response to perturbations. Earth Surface Dynamics, 8 (2), 261–274. https://doi.org/10.5194/esurf-8-261-2020

Schwanghart, W., & Scherler, D. (2014). TopoToolbox 2–MATLAB-based software for topographic analysis and modeling in Earth surface sciences. Earth Surface Dynamics, 2, 1–7. https://doi.org/10.5194/esurf-2-1-2014

Seward, D., & Burg, J. P. (2008). Growth of the Namche Barwa Syntaxis and associated evolution of the Tsangpo Gorge; constraints from structural and thermochronological data. Tectonophysics, 451, 282–289. https://doi.org/10.1016/j.tecto.2007.11.057

Shelef, E., & Goren, L. (2021). The rate and extent of wind-gap migration regulated by tributary confluences and avulsions. Earth Surface Dynamics, 9(4), 687–700. https://doi.org/10.5194/esurf-2021-11

Shi, F., Tan, X., Zhou, C., & Liu, Y. (2021). Impact of asymmetric uplift on mountain asymmetry: Analytical solution, numerical modeling, and natural examples. Geomorphology, 389, 107862. https://doi.org/10.1016/j.geomorph.2021.107862

Stock, J. D., & Montgomery, D. R. (1999). Geologic constraints on bedrock river incision using the stream power law. Journal of Geophysical Research: Solid Earth, 104, 4983–4993. https://doi.org/10.1029/98JB02139

Stokes, M. F., Goldberg, S. L., & Perron, J. T. (2018). Ongoing river capture in the Amazon, Geophysical Research Letters, 45, 5545–5552, https://doi.org/10.1029/2018GL078129

Wang, P., Scherler, D., Liu-Zeng, J., Mey, J., Avouac, J.P., Zhang, Y., et al. (2014). Tectonic control of Yarlung Tsangpo Gorge revealed by a buried canyon in Southern Tibet. Science, 346, 978–981. https://doi.org/10.1126/science.1259041

Wei, H. H., Wang, E. C., Wu, G. L. & Meng, K. (2016). No sedimentary records indicating southerly flow of the paleo-Upper Yangtze River from the First Bend in southeastern Tibet. Gondwana Research, 32, 93–104. https://doi.org/10.1016/j.gr.2015.02.006

Whipple, K. X. (2001). Fluvial landscape response time: How plausible is steady-state denudation?. American Journal of Science, 301(4–5), 313–325. https://doi.org/10.2475/ajs.301.4-5.313

Whipple, K., Forte, A., DiBiase, R., Gasparini, N., & Ouimet, W. (2017). Timescales of landscape response to divide migration and drainage capture: Implications for the role of divide mobility in landscape evolution. Journal of Geophysical Research: Earth Surface, 122, 248–273. https://doi.org/10.1002/2016JF003973

Willett, S. D., McCoy, S. W., Perron, J. T., Goren, L., & Chen, C. Y. (2014). Dynamic reorganization of river basins. Science, 343, 1248765.

https://doi.org/10.1126/science.1248765

Willett, S.D., Slingerland, R. & Hovius, N. (2001). Uplift, shortening, and steady state topography in active mountain belts. American Journal of Science, 301(4–5), 455–485. https://doi.org/10.2475/ajs.301.4-5.455

Willis, S. C., Nunes, M., Montana, C. G., Farias, I. P., Ortí, G., et al. (2010). The Casiquiare river acts as a corridor between the Amazonas and Orinoco river basins: biogeographic analysis of the genus Cichla. Molecular Ecology, 19(5), 1014–1030. https://doi.org/10.1111/j.1365-294X.2010.04540.x

Winemiller, K. O., López-Fernández, H., Taphorn, D. C., Nico, L. G., & Duque, A. B. (2008). Fish assemblages of the Casiquiare River, a corridor and zoogeographical filter for dispersal between the Orinoco and Amazon basins. Journal of Biogeography, 35(9), 1551–1563. https://doi.org/10.1111/j.1365-2699.2008.01917.x

Xie, Y., Kang, C., Chi, Y., Wu, P., Wei, Z., Wang, J., et al. (2020). Reversal of the middle upper Songhua River in the late Early Pleistocene, Northeast China. Geomorphology, 369(107373), 1–17. https://doi.org/10.1016/j.geomorph.2020.107373

Xing, Y. & Ree, R. H. (2017). Uplift-driven diversification in the Hengduan Mountains, a temperate biodiversity hotspot. Proceedings of the National Academy of Sciences, 114, E3444–E3451.

Yang, R., Herman, F., Fellin, M. G., & Maden, C. (2018). Exhumation and topographic evolution of the Namche Barwa Syntaxis, eastern Himalaya. Tectonophysics, 722, 43–52. https://doi.org/10.1016/j.tecto.2017.10.026

Yang, R., Herman, F., Liu, T., Biswas, R. H., Fellin, M. G., Tian, Y., et al. (2021). Enhanced Quaternary exhumation in the Namche Barwa syntaxis, eastern Himalaya. Geology, 49(8), 958–962. https://doi.org/10.1130/G48595.1

Yang, R., Suhail, H. A., Gourbet, L., Willett, S. D., Fellin, M. G., Lin, X., et al. (2020). Early Pleistocene drainage pattern changes in Eastern Tibet: Constraints from provenance analysis, thermochronometry, and numerical modeling. Earth and Planetary Science Letters, 531, 115955. https://doi.org/10.1016/j.epsl.2019.115955

Yang, R., Willett, S. D., & Goren, L. (2015). In situ low-relief landscape formation as a result of

river network disruption. Nature, 520(7548), 526–529. https://doi.org/10.1038/nature14354

Yanites, B. J., Ehlers, T. A., Becker, J. K., Schnellmann, M., & Heuberger, S. (2013). High magnitude and rapid incision from river capture: Rhine River, Switzerland. Journal of Geophysical Research: Earth Surface, 118, 1060–1084. https://doi.org/10.1002/jgrf.20056

Ye, Y., Tan, X., & Zhou, C. (2022). Initial topography matters in drainage divide migration analysis: Insights from numerical simulations and natural examples. Geomorphology, 409, 108266. https://doi.org/10.1016/j.geomorph.2022.108266

Yu, X. J., Ji, J. Q., Gong, J. F., Sun, D. X., Qing, J. C., Wang, L. N., et al. (2011). Evidences of rapid erosion driven by climate in the Yarlung Zangbo (Tsangpo) Great Canyon, the eastern Himalayan syntaxis. Chinese Science Bulletin, 56, 1123−1130. https://doi.org/10.1007/s11434-011-4419-x

Zeitler, P. K., Meltzer, A. S., Brown, L., Kidd, W. S. F., Lim, C., & Enkelmann, E. (2014). Tectonics and topographic evolution of Namche Barwa and the easternmost Lhasa Block. In: Nie, J., Hoke, G.D., Horton, B. (Eds.), Towards an Improved Understanding of Uplift Mechanisms and the Elevation History of the Tibetan Plateau. Standard Performance Evaluation Corporation, 507, 23–58.

Zeitler, P. K., Meltzer, A. S., Koons, P. O., Craw, D., Hallet, B., Chamberlain, C. P., et al. (2001). Erosion, Himalayan geodynamics, and the geomorphology of metamorphism. Geological Society of America Today, 11, 4–9. https://doi.org/10.1130/1052-5173(2001)0112.0.CO;2

Zeng, X., & Tan, X. (2023). Drainage divide migration in response to strike-slip faulting: An example from northern Longmen Shan, eastern Tibet. Tectonophysics, 229720. https://doi.org/10.1016/j.tecto.2023.229720

Zhang, J. Y., Yin, A., Liu, W., Wu, F., Lin, D., & Grove, M. (2012). Coupled U-Pb dating and Hf isotopic analysis of detrital zircon of modern river sand from the Yalu River (Yarlung Tsangpo) drainage system in southern Tibet: Constraints on the transport processes and evolution of Himalayan rivers. Geological Society of America Bulletin, 124, 1449–1473. https://doi.org/10.1130/B30592.1

Zhang, P., Najman, Y., Mei, L., Millar, I., Sobel, E. R., Carter, A., et al. (2019). Palaeodrainage evolution of the large rivers of East Asia, and Himalayan-Tibet tectonics. Earth-Science

Reviews, 192, 601–630. https://doi.org/10.1016/j.earscirev.2019.02.003

Zhao, X., Zhang, H., Hetzel, R., Kirby, E., Duvall, A. R., Whipple, K. X., et al. (2021b). Existence of a continental-scale river system in eastern Tibet during the late Cretaceous–early Palaeogene. Nature communications, 12(1), 7231. https://doi.org/10.1038/s41467-021-27587-9

Zhao, X., Zhang, H., Tao, Y., Wang, Y., Pang, J., Ma, Y., et al. (2021a). Pliocene to Early Pleistocene drainage reorganization in eastern Tibet inferred from detrital zircons. Geophysical Research Letters, 48, e2021GL094563. https://doi.org/10.1029/2021GL094563

Zheng, Y., Li, H., Pan, J., Gong, Z., Wang, P., Lai, Y., et al. (2023). Mid-Pleistocene drainage rearrangement of the Dadu River in response to plate convergence in southeastern Tibet. Quaternary Research, 114, 130-147. https://doi.org/10.1017/qua.2022.71

Zhou, C., Tan, X., Liu, Y., & Shi, F. (2022a). A cross-divide contrast index (C) for assessing controls on the main drainage divide stability of a mountain belt. Geomorphology 398, 108071. https://doi.org/10.1016/j.geomorph.2021.108071

Zhou, C., Tan, X., Liu, Y., Lu, R., Murphy, M. A., He, H., et al. (2022b). Ongoing westward migration of drainage divides in eastern Tibet, quantified from topographic analysis. Geomorphology, 402, 108123. https://doi.org/10.1016/j.geomorph.2022.108123

Zondervan, J. R., Stokes, M., Boulton, S. J., Telfer, M. W., & Mather, A. E. (2020). Rock strength and structural controls on fluvial erodibility: Implications for drainage divide mobility in a collisional mountain belt. Earth and Planetary Science Letters, 538, 116221. https://doi.org/10.1016/j.epsl.2020.116221